MATERIALS CHEMISTRY FRONTIERS

RESEARCH ARTICLE

View Article Online
View Journal | View Issue

Cite this: *Mater. Chem. Front.*, 2020, **4**, 1706

Each phenyl group performs its own functions on luminescence: phenyl substituted effect in tetraphenylpyrazine†

Haozhong Wu,[a] Xiaojuan Song,[b] Bing Zhang,[a] Zhiming Wang, *[a] Tian Zhang, *[b] Anjun Qin [a] and Ben Zhong Tang [ac]

Received 24th February 2020,
Accepted 6th April 2020

DOI: 10.1039/d0qm00098a

rsc.li/frontiers-materials

Aggregation-induced emission (AIE) has drawn considerable attention owing to its interesting phenomenon, and the AIE mechanisms of different molecule systems have been gradually revealed. Here, we investigated the difference in 3-carbazole-pyrazine-based isomers and explored the effects of three substituted phenyl groups (*ortho*, *meta* and *para*) on the tetraphenylpyrazine derivatives (TPPs). The *meta*- and *para*-phenyl groups could slightly and significantly adjust their emission properties, respectively. The *ortho*-phenyl group could distort the pyrazine plane owing to the large steric hinderance of the two moieties; this triggered many molecular motions and led to the wastage of excited state energy, stimulating the AIE characteristics of TPPs. This result is demonstrated for other pyrazine derivatives and can serve as a design strategy of AIE molecules.

Introduction

Organic π-conjugated fluorescent materials have been investigated in the past several decades owing to their promising applications in organic light-emitting diodes (OLEDs),[1–6] chemical sensors[7–11] and biological imaging.[12–17] However, the notorious problem of these classical luminescent materials is the familiar aggregation-caused quenching (ACQ), *i.e.*, they weakly emit in their aggregated states such as powder and crystals compared to their dilute solutions.[18] To overcome this issue, Tang *et al.* proposed the opposite phenomenon, namely, aggregation-induced emission (AIE). From then on, many AIE luminogens (AIEgens) have been explored and developed in multiple research fields.[19–22]

Compared to common fluorophores, AIEgens undergo some complicated relaxation paths in their excited states; therefore, several mechanisms, such as restricted intramolecular motions (RIMs) and that of J-aggregates, have been put forward to explain the AIE phenomenon. Among them, RIM has been widely acknowledged as one of the origins of AIE.[19,20,23–26] From single molecular states to aggregated states, the restricted moieties of different molecular systems are not identical (Fig. 1A–C). In dilute solutions, twisting double-bond of tetraphenylethene (TPE) and its derivatives can lead the potential energy surface to the conical intersection and return to the ground states without strong fluorescence.[27] For the TICT model compounds, the nearly perpendicular donor–acceptor structures hinder the radiative decay process because of less orbital overlap and accelerate internal crossing due to the small energy gaps.[28–31] The aromaticity reversal of cyclooctatetrathiophene produces many structural vibrations;[32] therefore, weak emissions can be observed in these molecules. Once aggregated, the restriction of all the abovementioned motions leads to bright fluorescence.

Tetraphenylpyrazine (TPP) has been discovered as an AIE unit; it is often considered that the obstruction of the rotation with respect to the peripheral phenyl groups leads to AIE features (Fig. 1D).[33] Lately, the X-ray diffraction of the crystalline structure and theoretical calculations have demonstrated that the pyrazine cores of TPP-based molecules have some distortion, which can create a number of vibrational motions in their excited states.[34] Furthermore, the conjugation along the substituted axis mostly determines the transition process for single substituted compounds and the off-axis phenyl groups can influence this slightly.[35] Therefore, it is important to investigate the role of each phenyl group on TPP for the

[a] *State Key Laboratory of Luminescent Materials and Devices, Center for Aggregation-Induced Emission, Key Laboratory of Luminescence from Molecular Aggregates of Guangdong Province, Guangzhou International Campus, South China University of Technology (SCUT), Guangzhou 510640, China. E-mail: wangzhiming@scut.edu.cn*

[b] *School of Chemistry and Chemical Engineering, Shandong University of Technology, Zibo 255049, P. R. China. E-mail: tzhang@sdut.edu.cn*

[c] *Department of Chemistry, The Hong Kong University of Science & Technology (HKUST), Clear Water Bay, Kowloon, Hong Kong, China. E-mail: tangbenz@ust.hk*

† Electronic supplementary information (ESI) available: Synthesis, characterization, TGA curves, DSC curves, CV curves PL spectra. CCDC 1976103 and 1976104. For ESI and crystallographic data in CIF or other electronic format see DOI: 10.1039/d0qm00098a

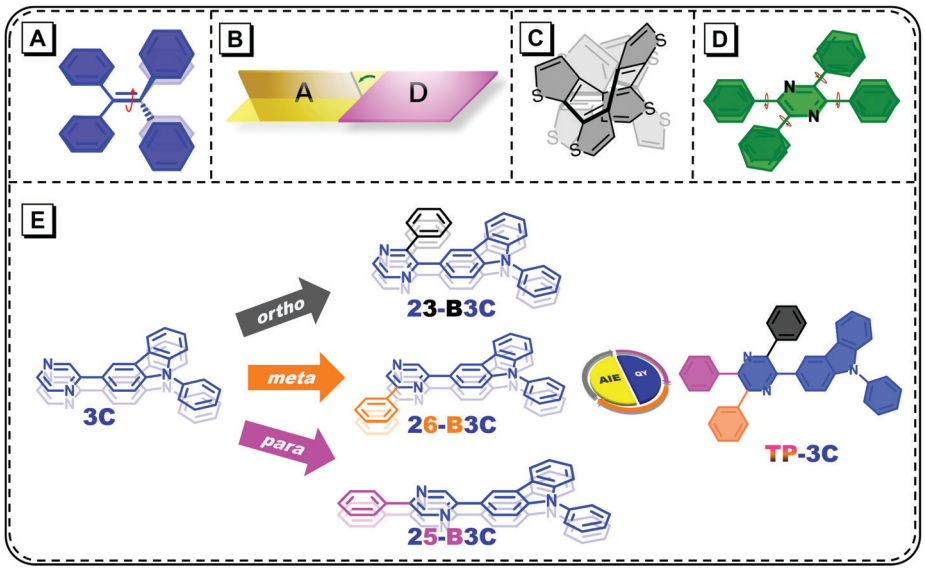

Fig. 1 The distortion modes of (A) TPE, (B) TICT molecules, (C) cyclooctatetrathiophene and (D) TPP; (E) the chemical structures of five pyrazine-carbazole derivatives.

further molecular design and modification. In this work, 3-carbazole was chosen as the chromophore owing to its rigidity and weak electron-donating ability. The phenyl group was introduced into the *ortho*, *meta* and *para* positions of pyrazine and three compounds, namely, 23-B3C, 26-B3C and 25-B3C were obtained, respectively. Also, a 3-carbazole-substituted compound 3C and a fully substituted compound TP-3C were synthesized for comparison (Fig. 1E).

Results and discussion

Synthesis and single crystal structure

The synthetic route of the five target products is outlined in Fig. S1 (ESI†). The details of the synthesis process and characterization are provided in the ESI† (Fig. S2–S15). 3C was prepared by a Suzuki coupling reaction with (9-phenyl-9*H*-carbazol-3-yl)boronic acid and 2-bromopyrazine. 23-B3C, 25-B3C and 26-B3C were also obtained from the corresponding dibromopyrazine, (9-phenyl-9*H*-carbazol-3-yl)boronic acid and phenylboronic acid *via* a Suzuki coupling reaction. TP-3C was obtained using 3-bromo-9-phenylcarbazole and was synthesized *via* the Sonogashira coupling reaction, oxidation reaction and Schiff base cycling reaction successively.[34] These final compounds were soluble in common organic solvents, such as tetrahydrofuran (THF) and dichloromethane, but not in methanol and water.

To investigate the substituted distinction on crystalline packing, we tried to prepare single crystals, but only 23-B3C (CCDC 1976103†) and 25-B3C (CCDC 1976104†) were obtained by evaporation from methanol/dichloromethane or methanol/THF mixtures. The detailed analysis of the resulting X-ray diffraction (XRD) data is shown in the ESI.† As illustrated in Fig. 2A, 23-B3C adopts a twisted conformation with a distortion of approximately 44° between pyrazine and 3-carbazole due to the steric hindrance between 3-carbazole and the phenyl group, which can prohibit the notorious π–π stacking in a manner similar to that of many classic AIEgens such as TPE and polyphenylsilole (Fig. 2A and E).[36] Some C–H···π intermolecular interactions are beneficial to restrict molecular motions (Fig. 2B). Hence, we supposed that 23-B3C had the AIE characteristic based on this molecular structure and packing pattern. Nevertheless, the large pyrazine-(3-carbazole) torsion angle indicated that weak fluorescence may be observed in its solid state. In the 25-B3C crystal, the strong C–H···π and C–H···N intermolecular interactions could also hinder the molecular motions (Fig. 2D); however, the torsion and packing situations were different. The small pyrazine-(3-carbazole) dihedral angle of 25-B3C (16°) can lead to slight face-to-face stacking with a distance of *ca.* 3.3 Å (Fig. 2C and F), which probably would not turn on its AIE activity. Because of the planar structure and no serious π–π stacking, relatively high fluorescence efficiency in the solid state might be expected in 25-B3C.

Photophysical properties

The photophysical properties of these five compounds were analyzed based on the absorption spectra and photoluminescence (PL) spectra. As shown in Fig. 3A, the molecule 3C exhibits strong absorption bands at 300–370 nm in a THF solution with a peak at 329 nm, corresponding to the π–π* transition of the whole skeleton; however, the absorption peaks of 26-B3C, TP-3C and 25-B3C shift to 334, 347 and 349 nm, respectively, because of their larger molecular conjugation. Interestingly, the molecular conjugation of 23-B3C was considered to be larger than that of 3C because of an additional phenyl group on 23-B3C compared to 3C; however, 23-B3C showed a slightly blue-shifted absorption profile compared with 3C, which may result from the twisted structure induced by the *ortho*-substituted phenyl group. Similarly, the absorption

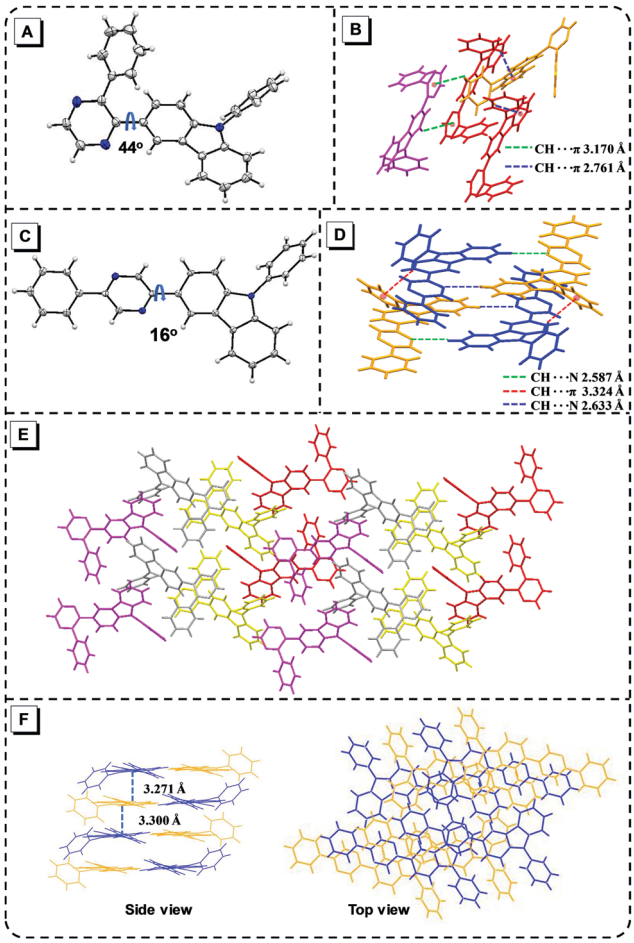

Fig. 2 Molecular structure in crystals of 23-B3C (A) and 25-B3C (C); intermolecular interactions in 23-B3C (B) and 25-B3C (D); crystal packing of 23-B3C (E) and 25-B3C (F).

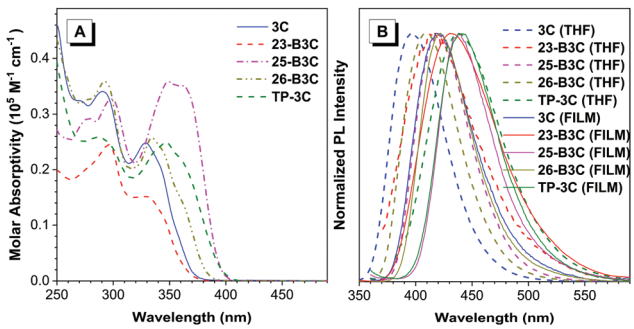

Fig. 3 (A) The absorption spectra of five compounds in THF solutions; (B) the PL spectra of five compounds in THF solutions and films.

peak of TP-3C (347 nm) was smaller than that of 25-B3C (349 nm) possibly because of its twisted structure. The series of pyrazine-based materials emitted violet and deep-blue fluorescence in both THF solutions and film states (Fig. 3B). For the 3-position substituted derivatives, 23-B3C and TP-3C showed weak emissions with fluorescence efficiency (Φ) values of 0.005 and 0.010 in THF solutions, while their Φ values were enhanced to 0.053 and 0.319 in film states, respectively (Table 1). For non-*ortho*-substituted compounds, enhancements in Φ were not observed with the states changing from solutions to films: 0.330, 0.793 and 0.396 in THF solutions and 0.134, 0.694 and 0.176 in film states for 3C, 25-B3C and 26-B3C, respectively; this indicated that the *ortho*-substituted compounds 23-B3C and TP-3C possessed AIE features, but substituting at either *meta* or *para* position did not endow 26-B3C and 25-B3C with classic AIE properties similar to the undecorated molecule 3C. Larger full width at half maximum (FWHM) values were observed for 23-B3C (75 nm) and TP-3C (76 nm) compared to other non-AIE active compounds (*ca.* 55 nm), which might indicate the flexibility of AIEgens. For *meta*-substituted derivatives, 26-B3C emitted slightly red-shifted fluorescence at 408 nm (0.396) and 421 nm (0.176) in THF solution and film state, respectively, while the PL spectra of the *para*-substituted 25-B3C were on the redder region with the emission peaks at 419 nm (0.793) in solution and 439 nm (0.694) in the film state. These results suggest that pyrazine compounds can be effectively tuned to obtain suitable fluorescence efficiency *via* inserting fluorophores at their *meta* positions; moreover, intense fluorescence can be observed with modifications at the *para* positions. For the triphenyl substituted situation, therefore, TP-3C integrates the PL performance from 23-B3C, 25-B3C and 26-B3C.

Their AIE nature was further validated through the investigation of the emission behaviors of the five compounds in THF/water mixtures (Fig. S16, ESI†). For 23-B3C, its PL intensity gradually decreased with the emission peak shifting to the long wavelength region until the water fraction (f_w, vol%) increased to 60% probably because of charge transfer (CT) emission.[37] After this, it dramatically increased as the unconstrained molecules transformed to nanoaggregates. For TP-3C, its PL intensity slowly increased with the increase in the water fraction but remained low when f_w was less than 60%, while it sharply increased when f_w was more than 60%. The bright emission in nanoaggregates is attributed to the obstruction of non-radiative decay channels by restricted intramolecular motions.[19] For non-AIE active compounds, 3C, 25-B3C and 26-B3C showed weaker fluorescence with the increase in f_w compared to pure THF, and this elucidated that *meta* and *para* substitution could not furnish AIE character again.

Theoretical calculations

As mentioned above, we speculate that substitution at three positions can achieve two effects; one is that bonding at the *ortho*-position can provide materials with AIE characteristics; the other is that insertion at the *meta*- or *para*-position can tune the emission wavelength and enhance fluorescence efficiency but cannot obtain AIE features. Herein, we chose 23-B3C and 25-B3C to discuss the AIE activity theoretically. The THF solution phase and aggregation effects were taken into account through the polarizable continuum model (PCM) and the combined quantum mechanics/molecular mechanics (QM/MM) approach, as implemented in the Gaussian 16 package. The geometrical structures were optimized by (time dependent) theoretical density functional ((TD)DFT) method with PBE0/6-31G(d) level. The natural

Table 1 The photophysical properties of five compounds

Compound	λ_{abs}[a] (nm)	λ_{em}[b] (nm)				Φ[c]		τ[d] (ns)		k_r[e] (10^7 s^{-1})		k_{nr}[f] (10^7 s^{-1})	
		Soln	FWHM	Film	FWHM	Soln	Film	Soln	Film	Soln	Film	Soln	Film
3C	329	397	55	420	52	0.330	0.134	1.70	2.29	19.4	5.9	39.4	37.8
23-B3C	328	415	75	430	78	0.005	0.053	0.96	1.37	0.5	3.9	103.6	69.1
25-B3C	349/363	419	57	439	55	0.793	0.694	1.86	1.46	42.6	47.5	11.1	21.0
26-B3C	334	408	56	421	54	0.396	0.176	2.42	1.95	16.4	9.0	25.0	42.3
TP-3C	347	437	76	440	61	0.010	0.319	0.88	0.71	1.1	44.9	112.5	95.9

[a] Maximum absorption wavelength, concentration: 10^{-5} M. [b] Maximum emission wavelength, soln: THF solution, film: neat film, FWHM: full width at half maximum. [c] Absolute fluorescence quantum efficiency. [d] Fluorescence lifetime. [e] $k_r = \Phi/\tau$. [f] $k_{nr} = (1 - \Phi)/\tau$.

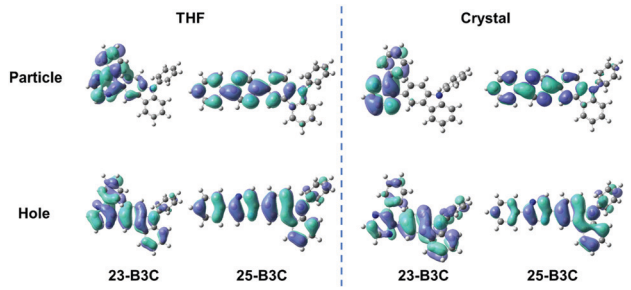

Fig. 4 The NTOs of 23-B3C and 25-B3C in THF solution and crystals.

transition orbitals (NTOs) were calculated to understand their electronic structure and all transition ratios from holes to particles were up to 99%. As displayed in Fig. 4, the holes of 23-B3C and 25-B3C are dispersed on the whole molecules, while their particles are mainly determined by pyrazine and conjoint phenyl groups in both THF solutions and crystal states. In addition, 23-B3C showed more obvious orbital separation in crystals than in THF solutions, which indicated more CT proportion in crystals as expected and resulted in faint fluorescence. For 25-B3C, no remarkable disparity of NTO separation could be distinguished between solution and crystal states; thus, it can effectively fluoresce in both solution and solid states.

The reorganization energies of 23-B3C and 25-B3C in both solution and crystal states were investigated. The low-frequency (LF, <200 cm^{-1}) and high-frequency (HF, 1400–1800 cm^{-1}) modes and the related contributions to the total reorganization energies were obtained by normal mode analyses (Fig. 5 and Table S1, ESI†). The LF modes mainly originated from the alteration of the dihedral angle by rotating phenyl and 3-carbazole groups, which could be hindered by molecular packing similar to many AIE compounds. The HF parts show the vibrations of intramolecular bonds and show little dependence on the stacking patterns.[34,38–40] In solution, the total reorganization energy of 23-B3C is evaluated to be 529 meV with 41% LF modes and 29% HF modes, indicating that many molecular rotations exist. In the crystal state, its total reorganization energy reduces to 329 meV and the LF part decreases to 46 meV from 218 meV. The large depression of the LF modes from solution to crystal states contributes to this AIE characteristic. Compared with the distinct reorganization energy change of 23-B3C, 25-B3C displays only 5 meV difference on the LF modes between THF solution and crystal and these modes are not more than a quarter of the total reorganization energy; thus, no AIE phenomenon for 25-B3C is rational.

The changes in the dihedral angles of 23-B3C and 25-B3C from ground states to excited states were studied and listed in Table 2. In THF solution, 23-B3C shows a large conformation adjustment on excitation, *e.g.*, 19.90° of $\Delta(\alpha_{1\text{-}2\text{-}3\text{-}4})$ but not for 25-B3C (0.86° of $\Delta(\alpha_{1\text{-}2\text{-}3\text{-}4})$). The difference between 23-B3C and 25-B3C implies that *ortho*-insertion can break pyrazine's planarity, reduce the rigidity and cause massive molecular motions. In crystals, all the changes in α decrease substantially, which demonstrates that the molecular rotations and pyrazine distortion are restrained, contributing to their AIE features.

Due to the lack of single crystal structures of 3C, 26-B3C and TP-3C, their electronic structures and reorganization energies were computed only in the THF solution phase. Both 3C and 26-B3C showed relatively separated NTOs, while the local excited state occurred for TP-3C (Fig. S17, ESI†). As illustrated in Fig. S18 (ESI†), the total reorganization energies of 3C and 26-B3C are just 219 and 240 meV, and the LF parts are only 35 and 48 meV, respectively, less than 20% of the total value, respectively. Additionally, their pyrazine cores are only slightly warped (Table S2, ESI†). Therefore, this implies that the good planarity of pyrazine also exists in 3C and 26-B3C and produces a little reorganization energy, which is advantageous for luminescence, similar to 25-B3C. However, in contrast to 25-B3C, an obvious fluorescence quenching effect was observed for 3C and 26-B3C probably because of the different stacking patterns that we could not investigate. On the contrary, TP-3C exhibited a considerably more reorganization energy of 406 meV and its LF section of 120 meV was larger than that of non-AIE molecules. The clear pyrazine's torsion was recorded in both S_0 and S_1 states, and it became more twisted after excitation (Table S2, ESI†); this indicated the undermining of the pyrazine's planarity because steric hinderance caused considerable energy waste for molecular motions, similar 23-B3C. In the solid state, the restriction of these motions led to the AIE phenomenon. Two more phenyl groups modified on 23-B3C could increase its conjugation and rigidity, which explained the smaller reorganization energy of TP-3C than that of 23-B3C; therefore, TP-3C could emit more efficiently than 23-B3C in both solution and solid states.

Demonstration of pyrazine's planarity and AIE

To validate this point, we changed the chromophore and synthesized three *ortho*-disubstituted pyrazine compounds,

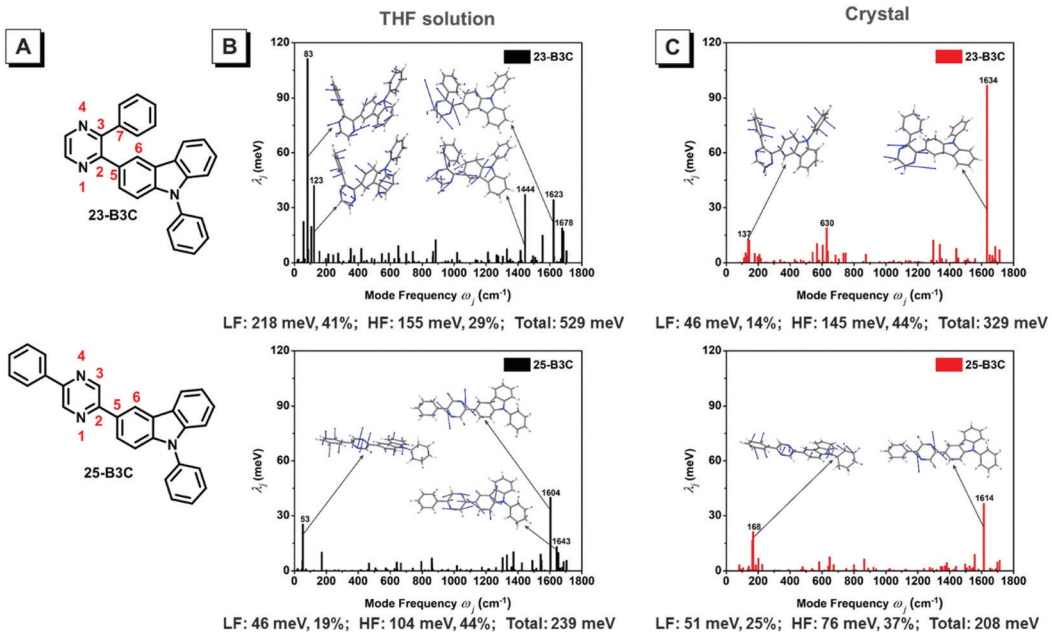

Fig. 5 (A) Atom label of 23-B3C and 25-B3C; the projection of the reorganization energy onto mode relaxations for two compounds (B) in THF solution and (C) crystals.

Table 2 The selected dihedral angles of 23-B3C and 25-B3C in THF solutions and crystals

		23-B3C			25-B3C	
		$\alpha_{1\text{-}2\text{-}3\text{-}4}$	$\alpha_{3\text{-}2\text{-}5\text{-}6}$	$\alpha_{5\text{-}2\text{-}3\text{-}7}$	$\alpha_{1\text{-}2\text{-}3\text{-}4}$	$\alpha_{1\text{-}2\text{-}5\text{-}6}$
THF	S_0	−8.88	−40.07	−12.46	−0.39	−17.74
	S_1	−28.78	−16.47	−39.55	0.47	−0.04
	Δ	19.90	−23.60	27.09	0.86	−17.70
Crystal	S_0	−6.85	−43.06	−9.81	−1.02	−15.08
	S_1	−8.09	−40.21	−14.50	−1.61	−10.68
	Δ	1.24	−2.85	4.69	0.59	−4.40

namely, P-2PF, HP-2PF and PP-2PF for the flexibility of the mechanism (Fig. S19–S27, ESI†). PP-2PF is the respective benzo-derivative of P-2PF, and HP-2PF is the non-conjugated derivative. Their geometries were computed first. As shown in Table S3 (ESI†), the $\Delta\alpha_{1\text{-}2\text{-}3\text{-}4}$ value of PP-2PF (3.32°) is smaller than that of P-2PF (16.91°); therefore, the pyrazine's planarity of PP-2PF is better than that of P-2PF. When pyrazine is transformed to benzopyrazine (also called quinoxaline), the electron-withdrawing feature will be strengthened; thus, the apparently separated orbital distribution was acquired (Fig. S28, ESI†). For HP-2PF, the structural change and NTOs were almost identical to those of P-2PF, which suggested that the non-conjugated modification did not affect its planarity. If pyrazine's planarity can be destroyed in the *ortho*-substituted mode and create numerous motions, considerable excited state energy will be consumed in the non-radiative relaxation path. As expected, P-2PF and HP-2PF showed obvious AIE, where the corresponding Φ values in THF were 0.022 and 0.021, which then increased to 0.186 and 0.157 in film states, respectively. PP-2PF with good planarity exhibited moderate AIE: 0.155 in THF and 0.419 in film state (Fig. S29, S30 and Table S4, ESI†). Therefore, these results demonstrate that the destruction of pyrazine's planarity leads to the AIE phenomenon.

Device characterization

Because of the suitable photoluminescence efficiency of 25-B3C, 26-B3C and TP-3C, we evaluated their electroluminescence (EL) performance. Previously, their thermal stability and morphological stability were tested by thermogravimetric analysis (TGA) and differential scanning calorimetry (DSC), respectively (Fig. S31, ESI†). We observed good thermal stability with temperatures of 5% weight loss (T_d) as high as 343, 315 and 386 °C and good morphological stability with the glass transition temperatures (T_g) of 60, 60 and 119 °C for 25-B3C, 26-B3C and TP-3C, respectively. Besides, the HOMO levels were determined from the onset of oxidation potential with the following equation: $E_{HOMO} = -(E_{onset} - E_{Fc/Fc^+} + 4.8)$ eV. The values of LUMOs were calculated using the following equation: $E_{HOMO} = E_{LUMO} + E_{gap}$, $E_{gap} = 1240/\lambda_{onset}$; here, E_{Fc/Fc^+} was 0.40 eV and λ_{onset} was calculated based on the onset of absorption in dichloromethane (Fig. S32, ESI†). As shown in Table S2 (ESI†), the HOMO values of 25-B3C, 26-B3C and TP-3C were estimated to be −5.59, −5.54, and −5.55 eV, respectively. Their corresponding LUMO energy levels were then calculated to be −2.42, −2.29, and −2.40 eV. It is feasible to apply them for blue emitters (Table S5, ESI†).

Non-doped and 20 wt%-doped OLED devices employing three materials as emitters with the configuration ITO/HATCN (5 nm)/TAPC (50 nm)/TCTA (5 nm)/EML (20 nm)/TmPyPB (40 nm)/LiF (1 nm)/Al (120 nm) were fabricated. In these devices, HATCN ((2,3,6,7,10,11-hexacyano-1,4,5,8,9,12-hexaazatriphe-nylene)) and TAPC (1,1-bis(4-di-*p*-tolylaminophenyl)cyclohexane) served

Table 3 EL performance of OLED devices

EML	λ_{EL} (nm)	V_{on} [b] (V)	L [a] (cd m^{-2})	η_c [a] (cd A^{-1})	η_P [a] (lm W^{-1})	EQE [a] (%)	CIE$_{(x, y)}$ [c]
25-B3C	436	3.3	1776	1.66	1.42	2.29	(0.15, 0.08)
26-B3C	420	2.9	1621	1.81	1.89	3.32	(0.16, 0.07)
TP-3C	452	3.3	1672	1.97	1.73	1.54	(0.19, 0.18)
CBP:20 wt% 25-B3C	424	3.3	1383	1.93	1.78	4.29	(0.16, 0.06)
CBP:20 wt% 26-B3C	412	2.9	1007	0.78	0.76	2.85	(0.16, 0.04)
CBP:20 wt% TP-3C	444	3.1	1907	2.15	1.99	2.69	(0.15, 0.10)

[a] The luminescence (L), current efficiency (η_c), power efficiency (η_P) and external quantum efficiency are the maximum values of the devices. [b] V_{on} is the turn-on voltage at 1 cd m^{-2}. [c] CIE coordinates at 10 mA cm^{-2}.

as the hole-injecting layer and hole-transporting layer, respectively. TCTA (4,4′,4″-tri-9-carbazolytriphenylamine) acted as the hole-transporting layer and electron-blocking layer, and TmPyPB (1,3,5-tri[(3-pyridyl)-phen-3-yl]benezene) functioned as both the electron-transporting layer and hole-blocking layer. CBP (4,4′-bis(carbazol-9-yl)biphenyl) was chosen as the host material.

As shown in Table 3 and Fig. 6A, these devices were turned on at a low voltage of 2.9–3.3 V, which was attributed to the excellent balance of carrier transport, and exhibited deep-blue to sky-blue electroluminescence emissions with peaks (λ_{EL}) from 412 to 452 nm. Both doped and non-doped devices of 26-B3C showed the bluest fluorescence in this work. Among the non-doped OLED devices, 26-B3C performed the best with L_{max} of 1621 cd m^{-2}, $\eta_{ext,max}$ of 3.32% and $\eta_{P,max}$ of 1.89 lm W^{-1} and deep-blue emission with CIE coordinates of (0.16, 0.07). Generally, doped blue OLED devices often display a blue-shifted EL spectrum compared to non-doped ones; therefore, the EL spectrum of the doped devices shifted to 424, 412 and 444 nm and the values of CIE$_y$ decreased to 0.06, 0.04 and 0.10 for 25-B3C, 26-B3C and TP-3C, respectively. In this work, the

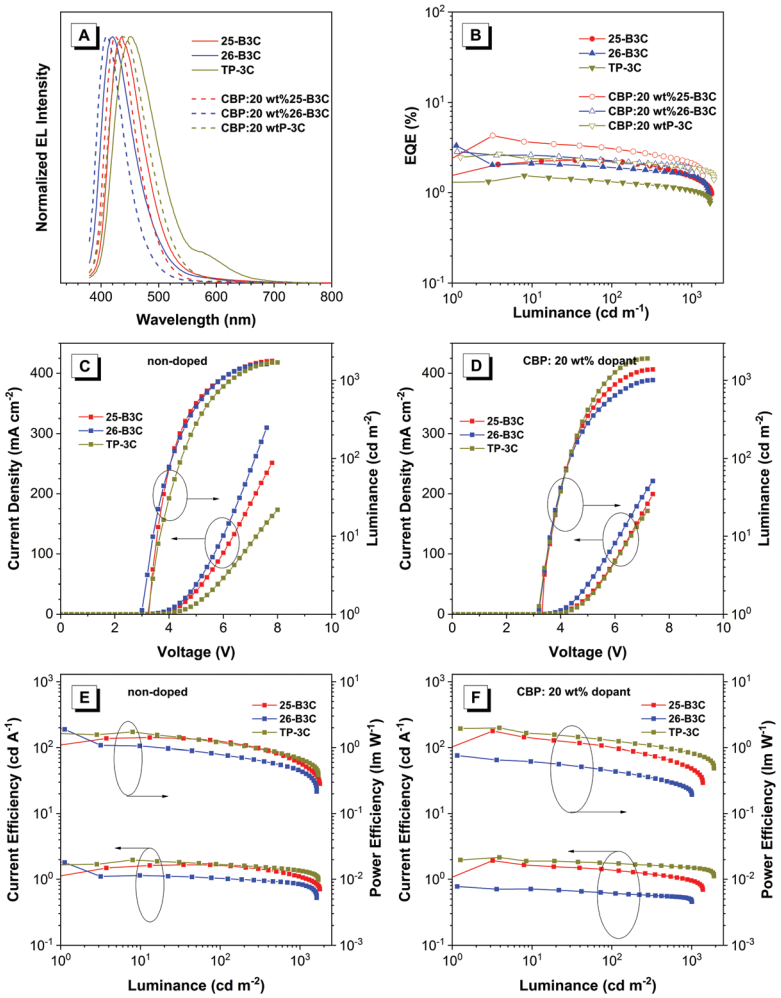

Fig. 6 The EL spectra, EQE–luminance, current density–voltage–luminance (J–V–L) and current efficiency–luminance–power efficiency curves for these non-doped and doped devices.

device of doped CBP:20 wt% 25-B3C showed the best EL efficiency: L_{max} of 1383 cd m^{-2}, $\eta_{P,max}$ of 1.78 lm W^{-1}, $\eta_{ext,max}$ of 4.29% and CIE coordinates of (0.16 0.06).

Conclusions

Blue pyrazine fluorophores with three different bonding positions (*ortho*, *meta* and *para*) were synthesized and the substituted effect was investigated. A phenyl group inserted on the *para* site (25-B3C) could increase molecular conjugation and generate strong emission with red-shifted spectra; however, *meta* substitution (26-B3C) could improve its PL efficiency and tune its fluorescence, slightly. Different from the substitution at *meta* and *para* positions, substitution at the *ortho* position (23-B3C) could provide pyrazine-carbazole derivatives with AIE features because the steric hindrance of the *ortho*-phenyl unit disturbed pyrazine's planarity and switched on the non-radiative process, which has been verified in other pyrazine and benzopyrazine derivatives. For highly effective luminescence, the doped OLED device based on CBP:20 wt% 25-B3C exhibited excellent deep-blue EL efficiency with an EQE of 4.29% and CIE coordinates of (0.16, 0.06). Therefore, high-efficiency luminescent materials can be exploited by this profound design.

Conflicts of interest

There are no conflicts to declare.

Acknowledgements

This work is financially supported by National Natural Science Foundation of China (21788102, 51673118, 21975077 and 21703122), Science & Technology Program of Guangzhou (201804010218 and 201804020027), the Innovation and Technology Commission of Hong Kong (ITC-CNERC14S01), the Fundamental Research Funds for the Central Universities (D2190960), Fund of Key Laboratory of Luminescence from Molecular Aggregates of Guangdong Province (2019B030301003) and the Natural Science Foundation of Shandong Province (ZR2017BB034).

Notes and references

1 T. M. Figueira-Duarte and K. Müllen, Pyrene-based materials for organic electronics, *Chem. Rev.*, 2011, **111**, 7260.
2 M. Zhu and C. Yang, Blue fluorescent emitters: design tactics and applications in organic light-emitting diodes, *Chem. Soc. Rev.*, 2013, **42**, 4963.
3 Y. Tao, K. Yuan, T. Chen, P. Xu, H. Li, R. Chen, C. Zheng, L. Zhang and W. Huang, Thermally activated delayed fluorescence materials towards the breakthrough of organoelectronics, *Adv. Mater.*, 2014, **26**, 7931.
4 R. Ieuji, K. Goushi and C. Adachi, Triplet-triplet upconversion enhanced by spin-orbit coupling in organic light-emitting diodes, *Nat. Commun.*, 2019, **10**, 5283.
5 Y. Kondo, K. Yoshiura, S. Kitera, H. Nishi, S. Oda, H. Gotoh, Y. Sasada, M. Yanai and T. Hatakeyama, Narrowband deep-blue organic light-emitting diode featuring an organoboron-based emitter, *Nat. Photonics*, 2019, **13**, 678.
6 A. Zampetti, A. Minotto and F. Cacialli, Near-infrared (NIR) organic light-emitting diodes (OLEDs): challenges and opportunities, *Adv. Funct. Mater.*, 2019, **29**, 1807623.
7 J. Y. Zheng, Y. Yan, X. Wang, W. Shi, H. Ma, Y. S. Zhao and J. Yao, Hydrogen peroxide vapor sensing with organic core/sheath nanowire optical waveguides, *Adv. Mater.*, 2012, **24**, OP194.
8 M. Denis, J. Pancholi, K. Jobe, M. Watkinson and S. M. Goldup, Chelating rotaxane ligands as fluorescent sensors for metal ions, *Angew. Chem., Int. Ed.*, 2018, **57**, 5310.
9 L. Zhang, X. A. Liu, K. D. Gillis and T. E. Glass, A high-affinity fluorescent sensor for catecholamine: application to monitoring norepinephrine exocytosis, *Angew. Chem., Int. Ed.*, 2019, **58**, 7611.
10 R. Kumar, A. Sharma, H. Singh, P. Suating, H. S. Kim, K. Sunwoo, I. Shim, B. C. Gibb and J. S. Kim, Revisiting fluorescent calixarenes: from molecular sensors to smart materials, *Chem. Rev.*, 2019, **119**, 9657.
11 S.-N. Lei, H. Xiao, Y. Zeng, C.-H. Tung, L.-Z. Wu and H. Cong, BowtieArene: a dual macrocycle exhibiting stimuli-responsive fluorescence, *Angew. Chem., Int. Ed.*, 2019, **59**, 2.
12 B. A. D. Neto, P. H. P. R. Carvalho and J. R. Correa, Benzothiadiazole derivatives as fluorescence imaging probes: beyond classical scaffolds, *Acc. Chem. Res.*, 2015, **48**, 1560.
13 X. Xiong, F. Song, J. Wang, Y. Zhang, Y. Xue, L. Sun, N. Jiang, P. Gao, L. Tian and X. Peng, Thermally activated delayed fluorescence of fluorescein derivative for time-resolved and confocal fluorescence imaging, *J. Am. Chem. Soc.*, 2014, **136**, 9590.
14 A. Zhu, K. Miao, Y. Deng, H. Ke, H. He, T. Yang, M. Guo, Y. Li, Z. Guo, Y. Wang, X. Yang, Y. Zhao and H. Chen, Dually pH/reduction-responsive vesicles for ultrahigh-contrast fluorescence imaging and thermo-chemotherapy-synergized tumor ablation, *ACS Nano*, 2015, **9**, 7874.
15 P. Agarwal, B. J. Beahm, P. Shieh and C. R. Bertozzi, Systemic fluorescence imaging of zebrafish glycans with bioorthogonal chemistry, *Angew. Chem., Int. Ed.*, 2015, **54**, 11504.
16 C. Yin, X. Zhen, H. Zhao, Y. Tang, Y. Ji, Y. Lyu, Q. Fan, W. Huang and K. Pu, Amphiphilic semiconducting oligomer for near-infrared photoacoustic and fluorescence imaging, *ACS Appl. Mater. Interfaces*, 2017, **9**, 12332.
17 X. Wang, P. Li, Q. Ding, C. Wu, W. Zhang and B. Tang, Observation of acetylcholinesterase in stress-induced depression phenotypes by two-photon fluorescence imaging in the mouse brain, *J. Am. Chem. Soc.*, 2019, **141**, 2061.
18 G. v. Bünau, in *Photophysics of aromatic molecules*, ed. J. B. Birks, Wiley, London, 1970.
19 J. Mei, N. L. C. Leung, R. T. K. Kwok, J. W. Y. Lam and B. Z. Tang, Aggregation-induced emission: together we shine, united we soar!, *Chem. Rev.*, 2015, **115**, 11718.
20 S. Xu, Y. Duan and B. Liu, Precise molecular design for high-performance luminogens with aggregation-induced emission, *Adv. Mater.*, 2020, **32**, 1903530.

21 R. Núñez, M. Tarrés, A. Ferrer-Ugalde, F. F. de Biani and F. Teixidor, Electrochemistry and photoluminescence of icosahedral carboranes, boranes, metallacarboranes, and their derivatives, *Chem. Rev.*, 2016, **116**, 14307.
22 A. V. Marsh, N. J. Cheetham, M. Little, M. Dyson, A. J. P. White, P. Beavis, C. N. Warriner, A. C. Swain, P. N. Stavrinou and M. Heeney, Carborane-induced excimer emission of severely twisted bis-o-carboranyl chrysene, *Angew. Chem., Int. Ed.*, 2019, **57**, 10640.
23 Y. Hong, J. W. Y. Lam and B. Z. Tang, Aggregation-induced emission: phenomenon, mechanism and applications, *Chem. Commun.*, 2009, 4332.
24 Z. Liu, Z. Jiang, M. Yan and X. Wang, Recent progress of BODIPY dyes with aggregation-induced emission, *Front. Chem.*, 2019, **7**, 712.
25 X.-F. Zhang, Q. Xi and J. Zhao, Fluorescent and triplet state photoactive J-type phthalocyanine nano assemblies: controlled formation and photosensitizing properties, *J. Mater. Chem.*, 2010, **20**, 6726.
26 J. Shi, L. E. A. Suarez, S.-J. Yoon, S. Varghese, C. Serpa, S. Y. Park, L. Lüer, D. Roca-Sanjuán, B. Milián-Medina and J. Gierschner, Solid state luminescence enhancement in π-conjugated materials: unravelling the mechanism beyond the framework of AIE/AIEE, *J. Phys. Chem. C*, 2017, **121**, 23166.
27 K. Kokado and K. Sada, Consideration of molecular structure in the excited state to design new luminogens with aggregation-induced emission, *Angew. Chem., Int. Ed.*, 2019, **58**, 8632.
28 C. Wang, Q. Qiao, W. Chi, J. Chen, W. Liu, D. Tan, S. McKechnie, D. Lyu, X.-F. Jiang, W. Zhou, N. Xu, Q. Zhang, Z. Xu and X. Liu, Quantitative design of bright fluorophores and AIEgens via the accurate prediction of twisted intramolecular charge transfer (TICT), *Angew. Chem., Int. Ed.*, 2020, DOI: 10.1002/anie.201916357.
29 X. Liu, Q. Qiao, W. Tian, W. Liu, J. Chen, M. J. Lang and Z. Xu, Aziridinyl fluorophores demonstrate bright fluorescence and superior photostability by effectively inhibiting twisted intramolecular charge transfer, *J. Am. Chem. Soc.*, 2016, **138**, 6960.
30 Y. Luo, Y. Wang, S. Chen, N. Wang, Y. Qi, X. Zhang, M. Yang, Y. Huang, M. Li, J. Yu, D. Luo and Z. Lu, Facile access to twisted intramolecular charge-transfer fluorogens bearing highly pre-twisted donor-acceptor systems together with readily fine-tuned charge-transfer characters, *Small*, 2017, **13**, 1604113.
31 J. Li, C. Yang, X. Peng, Y. Chen, Q. Qi, X. Luo, W.-Y. Lai and W. Huang, Stimuli-responsive solid-state emission from *o*-carborane-tetraphenylethene dyad induced by twisted intramolecular charge transfer in the crystalline state, *J. Mater. Chem. C*, 2018, **6**, 19.
32 Z. Zhao, X. Zheng, L. Du, Y. Xiong, W. He, X. Gao, C. Li, Y. Liu, B. Xu, J. Zhang, F. Song, Y. Yu, X. Zhao, Y. Cai, X. He, R. T. K. Kwok, J. W. Y. Lam, X. Huang, D. L. Phillips, H. Wang and B. Z. Tang, Non-aromatic annulene-based aggregation-induced emission system via aromaticity reversal process, *Nat. Commun.*, 2019, **10**, 2952.
33 M. Chen, L. Li, H. Nie, J. Tong, L. Yan, B. Xu, J. Z. Sun, W. Tian, Z. Zhao, A. Qin and B. Z. Tang, Tetraphenylpyrazine-based AIEgens: facile preparation and tunable light emission, *Chem. Sci.*, 2015, **6**, 1932.
34 L. Pan, H. Wu, J. Liu, K. Xue, W. Luo, P. Chen, Z. Wang, A. Qin and B. Z. Tang, Tetraphenylpyrazine based AIE luminogens: unique excited state decay and its application in deep-blue light-emitting diodes, *Adv. Opt. Mater.*, 2019, **7**, 1801673.
35 H. Wu, J. Zeng, Z. Xu, B. Zhang, H. Zhang, Y. Pan, Z. Wang, D. Ma, A. Qin and B. Z. Tang, Triphenylpyrazine: methyl substitution to achieve deep blue AIE emitters, *J. Mater. Chem. C*, 2019, **7**, 13047.
36 Q. Li and Z. Li, The strong light-emission materials in the aggregated state: what happens from a single molecule to the collective group, *Adv. Sci.*, 2017, **4**, 1600484.
37 J. Mei, Y. Hong, J. W. Y. Lam, A. Qin, Y. Tang and B. Z. Tang, Aggregation-induced emission: the whole is more brilliant than the parts, *Adv. Mater.*, 2014, **26**, 5429.
38 X. Zheng, Q. Peng, L. Zhu, Y. Xie, X. Huang and Z. Shuai, Unraveling the aggregation effect on amorphous phase AIE luminogens: a computational study, *Nanoscale*, 2016, **8**, 15173.
39 M. Chen, X. Hu, J. Liu, B. Li, N. L. C. Leung, L. Viglianti, T. S. Cheung, H. H. Y. Sung, R. T. K. Kwok, I. D. Williams, A. Qin, J. W. Y. Lam and B. Z. Tang, Rational design of red AIEgens with a new core structure from non-emissive heteroaromatics, *Chem. Sci.*, 2018, **9**, 7829.
40 Y.-C. Duan, Y. Wu, J.-L. Jin, D.-M. Gu, Y. Geng, M. Zhang and Z.-M. Su, Influence of aggregation on the structure and fluorescent properties of a tetraphenylethylene derivative: a theoretical study, *ChemPhysChem*, 2017, **18**, 755.